Adaptive FTN Signaling Over Rapidly-Fading Channels

Mingfei Tong, Xiaojing Huang, *Senior Member, IEEE,*
J. Andrew Zhang, *Senior Member, IEEE,* and Lajos Hanzo, *Fellow, IEEE*

***Abstract*—The research of faster-than-Nyquist (FTN) signaling has reached a state of maturity for considering practical multipath fading channels, rather than idealized additive white Gaussian noise channels only. To overcome fast-fading multipath propagations, conventional FTN systems tend to rely on channel coding techniques for cleaning up the residual errors, rather than harnessing Doppler effect mitigation. To circumvent this limitation, we propose an adaptive transmit precoding (ATPC) method associated with FTN signaling for applications in fast-fading multipath channels. Upon leveraging real-time channel state information fed back by the receiver, ATPC updates the modulation matrix to improve resilience against Doppler frequency shifts. To mitigate the inter-block interference and multipath effect, a cyclic prefix is inserted at the beginning of each transmission frame. In addition, we employ decision-directed successive interference cancellation for alleviating the inter-symbol interference stemming from FTN signaling and multipath effects. We also analyze the theoretical bit error rate (BER) performance and a pair of closed-form BER expressions are derived for extreme channel conditions, i.e., sufficiently large number of paths and sufficiently large Doppler frequency shift. Simulation results verify the effectiveness of the proposed ATPC method and demonstrate our performance improvements over conventional schemes.**

***Index Terms*—FTN signaling, multipath fast-fading channel, delay-Doppler domain, inter-symbol interference, ATPC, and diversity order.**

I. Introduction

WITH the emergence of the sixth generation (6G) mobile communications era, attaining high spectral efficiency constitutes a fundamental requirement for new technology development. Among the promising techniques to be potentially employed in 6G systems, faster-than-Nyquist (FTN) signaling stands out in terms of enhancing the spectral efficiency. By increasing the transmission rate beyond the Nyquist rate, FTN enables the transmission of about 25% more bits within the same bandwidth, without compromising the bit-error-rate (BER) [1]. However, due to the symbol overlapping at sampling instants, the neighboring symbols will introduce inter-symbol interference (ISI) that poses a challenge for accurate data recovery. Hence, the mitigation of ISI represents a crucial aspect of FTN research and development.

Most of the previous FTN research only considered additive white Gaussian noise (AWGN) channels [2]–[9], rather than practical dispersive fading channels. For example, in [9], the performance vs. complexity aspects of time domain (TD) maximum-likelihood sequence estimation (MLSE) and frequency domain (FD) minimum mean square error (MMSE) equalization are investigated for transmission over AWGN channels, where the channel matrix is in Toeplitz form. While considering multipath fading channels, TD detection commonly applies a maximum $a\ posteriori$ (MAP) criterion based message passing algorithm (MPA), which introduces further complexity. FD detection typically suffers in the face of dynamically fluctuating channel state information (CSI). In the study of such multipath fading channels, the attainable diversity order constitutes a salient metric for evaluating the system's ability to recover the transmitted signals. The associated "degree of freedom" is also of pivotal significance in terms of quantifying the average pairwise error probability (PEP) [10]. Ideally, the system should attain full diversity order for high-integrity recovery of the transmitted signals. However, conventional FTN schemes cannot achieve full diversity due to the non-orthogonal signaling, which will degrade the reliability of data recovery. Therefore, it is imperative to conceive techniques capable of enhancing the diversity order or mitigating the adverse effects of multipath transmission.

FTN can be also combined with other advanced technologies, such as multiple-input-multiple-output (MIMO) and non-orthogonal multiple access (NOMA). The capacity of the FTN-MIMO systems operating in doubly-selective channels has been analyzed in [11] and [12]. However, these treatises are theoretically based rather than aiming for designing a tangible ISI cancellation algorithm applicable in practice. On the other hand, the iterative algorithms, proposed in [13] and [14] for FTN sparse code multiple access (SCMA) and FTN-NOMA systems, are complex due to their MPA-based iterative nature, hence posing significant challenges in practical applications.

When considering multipath scenarios, with the aid of channel coding, many of the conventional ISI cancellation schemes perform well. More explicitly, the truncated Bahl-Cocke-Jelinek-Raviv (BCJR) algorithm [15], FD equalization (FDE) [16]–[18], the turbo soft detector of [19], [20] and the expectation propagation based decoder of [21], are all capable of approaching the performance under AWGN channels. Additionally, joint channel estimation and equalization [22] is also capable of accurate CSI acquisition with the aid of channel coding. However, complexity reduction is a major challenge in such coded cases. In [23], both the ISI and inter-carrier interference (ICI) vectors are truncated and the equivalent interference matrix is eigenvalue-decomposed for reducing the

Mingfei Tong, Xiaojing Huang, and J. Andrew Zhang are with the Global Big Data Technologies Center, University of Technology Sydney, Australia (emails: Mingfei.Tong@student.uts.edu.au; Xiaojing.Huang@uts.edu.au; Andrew.Zhang@uts.edu.au). Lajos Hanzo is with the School of Electronics and Computer Science, University of Southampton, Southampton SO17 1BJ, U.K. (e-mail: lh@ecs.soton.ac.uk).

complexity.

The above-mentioned treatises mostly aim for designing efficient interference cancellation methods for the receiver, but their powerful channel coding methods, such as turbo coding and low-density parity-check (LDPC) coding, further increase the complexity. For mitigating these problems, precoders [24]–[28] or pre-equalizers [29] have been proposed. According to [30], the design of the transceiver is relatively simple, and the weight matrix of the precoder can be obtained at the receiver. In [29], a linear pre-equalizer is proposed for reducing the ISI and a spectral precoder is added before it to avoid spectral broadening. Ishihara and Sugiura apply an eigenvalue-decomposition-based precoder for optimal power allocation and for further improving the BER in frequency-selective channels [24]–[26]. In [27], Li $et\ al.$ propose a precoding-based channel estimation and data detection method for enhancing the system performance. Wang $et\ al.$ propose an adaptive FTN scheme for dynamically adjusting mapping order, code rate and sampling rate [28]. These transmit-side methods open a new direction in reducing the complexity of ISI cancellation and improving the system capacity. However, the significance of achieving full-diversity transmission without channel coding is not considered in the above studies. Further research is required to investigate novel transmit-side techniques for uncoded FTN transmissions to combat fast fading, rather than solely relying on introducing brute-force redundancy into the transmitted information stream.

It is worth noting that in dispersive Rayleigh channels, the number of independently fading multipath components determines the diversity orders if each path shares equal power. However, in more practical non-line-of-sight (NLOS) and line-of-sight (LOS) channels, the power of each multipath component is different and time-varying, thus the diversity analysis will become far more complex. The diversity order has been analyzed for both orthogonal frequency-division multiplexing (OFDM) [31] as well as for single-carrier frequency-domain equalization (SC-FDE) [10] and for orthogonal time frequency space (OTFS) [32], [33] systems. However, the diversity analysis of FTN systems is unavailable in the open literature. To address this research gap, we systematically investigate the feasibility of combining FTN signaling with OFDM, SC-FDE and OTFS modulation schemes and assess their capabilities to achieve time-diversity and frequency-diversity, when considering both time-varying and frequency-selective fading scenarios.

In fast-fading multipath channels, the deleterious effects of Doppler frequency shift lead to frequency uncertainty and to continuously time-varying CSI [34], which aggravates the challenge of both equalization and interference cancellation. Therefore, eliminating the Doppler effect is a crucial prerequisite for high-integrity FTN data recovery. To solve this problem, we adopt an eigenvalue-decomposition-based adaptive transmit precoding (ATPC) method at the transmitter side. This method is designed for ensuring that the output signal-to-noise ratio (SNR) after channel equalization is optimized and the Doppler effect is removed. In this case, the ISI can be further mitigated by a successive interference cancellation algorithm [35]. Furthermore, we derive the BER performance of the adaptive FTN system considered. For performance benchmarking, we explore the diversity conditions related to two fundamental parameters: the number P of multipath components and the number K_{max} of maximum resolvable Doppler frequencies. For the two extreme channel conditions associated with $K_{max} = 0$ and $K_{max} \to \infty$, a pair of closed-form BER expressions are derived, respectively.

Besides Doppler effect, the multipath propagation channel introduces ISI that differs from FTN-ISI in terms of its statistics. These two types of ISI are distinct in the following aspects: First, FTN signaling induces ISI due to the loss of orthogonality between basis functions, such as those in Fourier transforms, whereas the ISI from the propagation channel arises when the delay spread exceeds the symbol period. Second, the FTN-ISI is deliberate and controllable, as a cost of achieving higher spectrum efficiency, while the ISI from the multipath propagation channel is random and time-varying. In this paper, these two types of ISI are jointly suppressed by the DDSIC algorithm.

Based on the signal models and the TPC method of [33], we study adaptive FTN signaling for transmission over rapidly fading channels. The differences between this paper and [33] are highlighted as follows: This paper introduces the TPC method to convert fast-fading expressions to slow-fading ones, enabling efficient FTN interference cancellation. By contrast, [33] uses TPC only for theoretical diversity performance analysis in conventional systems. This paper also considers new signal models in conjunction with FTN-specific parameters and presents novel algorithms as well as analytical results with the aid of the SNR expressions derived that consider the ISI imposed by FTN transmission and its implementation. Additionally, this paper approves that the equivalent modulation matrix after ATPC ensures minimized BER, which is absent in [33], justifying the correctness of the method.

The detailed novelties of this paper are explicitly contrasted to the existing literature in Table I. The most significant contributions of this paper are three-fold:

- Firstly, an adaptive FTN transmission system is proposed for achieving both time- and frequency-diversity with improved spectral efficiency in fast-fading multipath channels in the face of Doppler frequency shift in each path. This is also the first paper on FTN signaling aided OTFS.
- Secondly, the BER performance of the proposed FTN transmission over fast-fading multipath channels is analyzed. It is shown that the proposed ATPC method is capable of mitigating the Doppler effect and converting fast-fading to equivalent slow-fading channels. Decision-directed successive interference cancellation (DDSIC) is then shown to further mitigate the ISI. caused by FTN transmission. Moreover, simulation results demonstrate the robustness of the proposed scheme in two imperfect transmission scenarios: one involving fractional time delays and Doppler shifts, and the other concerning imperfect CSI feedback.
- Thirdly, the approximate eigenvalue probability density functions (PDFs) of the FTN channel matrix are derived under a pair of extreme channel conditions based on

TABLE I: COMPARISON OF FAST-FADING EFFECTS MITIGATION TECHNIQUES

Feature	[13]	[16]	[23]	[28]	[29]	[33]	This Paper
Dealing with Fast-Fading Channels				✔		✔	✔
Independent of Channel Coding		✔			✔	✔	✔
FTN Specific ISI Cancellation	✔	✔	✔	✔	✔		✔
Applying Transmit-Side Methodology				✔	✔	✔	✔
Applicable to OTFS-Type Modulation						✔	✔
Analytical Performance Benchmarking						✔	✔

the eigenvalue PDFs of a conventional full-rank channel matrix under the same extreme conditions. A pair of closed-form BER expressions are also derived, providing a useful theoretical base for benchmarking FTN systems communicating over fast-fading multipath channels.

The rest of this paper is organized as follows. In Section II, the structure of the proposed adaptive FTN scheme and the FD received signal model are introduced. The feasibility of combining FTN with three conventional modulation techniques of different time- and/or frequency-diversity is also discussed. In Section III, we introduce an ATPC method for mitigating the Doppler effect and analyze the BER performance of the proposed system. Based on the BER analysis, closed-form BER expressions are derived in Section IV for a pair of extreme cases. Simulation results are provided in Section V to verify the theoretical analyses and the feasibility of DDSIC under practical rapidly-fading multipath channels assisted by ATPC. Finally, we offer our conclusions in Section VI.

II. System Model and Modulation Schemes

In this section, the proposed adaptive FTN scheme and the associated modulation techniques are presented.

A. FTN System Model Relying on ATPC

Considering a single-input-single-output (SISO) system, Fig. 1 presents the architecture of our proposed adaptive FTN transmission system based on FD precoding using CSI feedback.

At the transmitter side, the input data bits are first mapped to Gray-coded quadrature amplitude modulated (QAM) constellation points. The mapped data symbols $x[i], i = 0, 1., , , MN-1$, are subsequently vectorized into an $MN \times 1$ vector $\mathbf{x} = (x[0], ..., x[MN-1])^T$, where M represents the number of subcarriers, N is the number of symbols per subcarrier, and $(\cdot)^T$ is the transpose of a matrix. Symbols are then accelerated to an interval of αT and processed by the $\mathbf{V}$-modulation module.

Among the associated modulation techniques, OTFS can be regarded as a general $\mathbf{V}$-modulation method, which is a precoded OFDM scheme [33]. In this paper, FTN detection is performed in the FD, and the Doppler effect of fast-fading channels leads to a time-varying CSI, which makes direct ISI cancellation and decision a challenge. To solve this problem, the conventional modulation module is converted to an ATPC module before FTN signaling in order to mitigate the Doppler effect: ATPC relying on the feedback matrix $\mathbf{Q}$ is employed. The ATPC is based on the ATPC weights gleaned from the CSI and will be elaborated on in Section III.C. Note that the cascade of the fast Fourier transform (FFT) matrix $\mathbf{F}_{MN}$, feedback matrix $\mathbf{Q}$, and the inverse fast Fourier transform (IFFT) matrix $\mathbf{F}_{MN}^{\mathbf{H}}$ can be interpreted as an updated modulation matrix $\mathbf{V} = \mathbf{F}_{MN}^{\mathbf{H}}\mathbf{Q}\mathbf{F}_{MN}$ while ATPC is employed. The data symbols to be transmitted can be expressed as $\mathbf{s} = \mathbf{V}\mathbf{x}$, where $\mathbf{s} = [s_0, s_1, ..., s_{MN-1}]^T$. Upon representing the modulation module by the matrix $\mathbf{V}$, the OFDM, SC-FDE, OTFS and ATPC signals can be constructed upon selecting different $\mathbf{V}$ matrices:

- For $N = 1, \mathbf{V} = \mathbf{F}_M^{\mathbf{H}}$ and $\mathbf{V} = \mathbf{I}_M$ represent OFDM and SC-FDE signals, respectively. Since the frame lengths of OFDM and SC-FDE are both M plus some signaling overhead, we refer to them as short-frame modulation schemes.
- For $N > 1, \mathbf{V} = \mathbf{F}_N^{\mathbf{H}} \otimes \mathbf{I}_M$ represents OTFS signals, where $\otimes$ denotes the Kronecker product. Since ATPC-OTFS has a frame length of MN plus the same signaling overhead, we refer to it as long-frame modulation.
- When the ATPC method is applied, the two modulation schemes are respectively converted to two new adaptive schemes, and the modulation matrix $\mathbf{V}$ remains unchanged, i.e., $\mathbf{V} = \mathbf{F}_{MN}^{\mathbf{H}}\mathbf{Q}\mathbf{F}_{MN}$. The only difference between these two schemes is the frame length.

To mitigate the inter-block interference (IBI), a cyclic prefix (CP), is concatenated after IFFT, and then these signals are passed through an RRC filter having the roll-off factor β and 3 dB cut-off bandwidth of $1/T$, where T is the symbol interval of Nyquist rate transmission. The transmitted FTN signals are expressed as

$$s(t) = \sum_{i=0}^{MN-1} s_i c(t - i\alpha T), 0 < \alpha < 1, \tag{1}$$

where s_i denotes the i-th precoded data symbol having average power of σ_s^2, $i = 0, 1, 2, ..., MN-1$, and $c(t)$ is the unit-energy RRC shaping pulse.

After the RRC pulse shaping, the signals are transmitted through a fast-fading multipath channel obeying a model similar to that in [33]. This model is characterized by a delay-Doppler spreading function $h(\tau, \nu)$ defined as

$$h(\tau, \nu) = \sum_{i=1}^{P} h_i c(\tau - \tau_i) g(\nu - \nu_i), \tag{2}$$

where h_i, τ_i and ν_i represent the channel gain, delay and Doppler shifts, respectively, $g(\cdot)$ is a sinc function defined

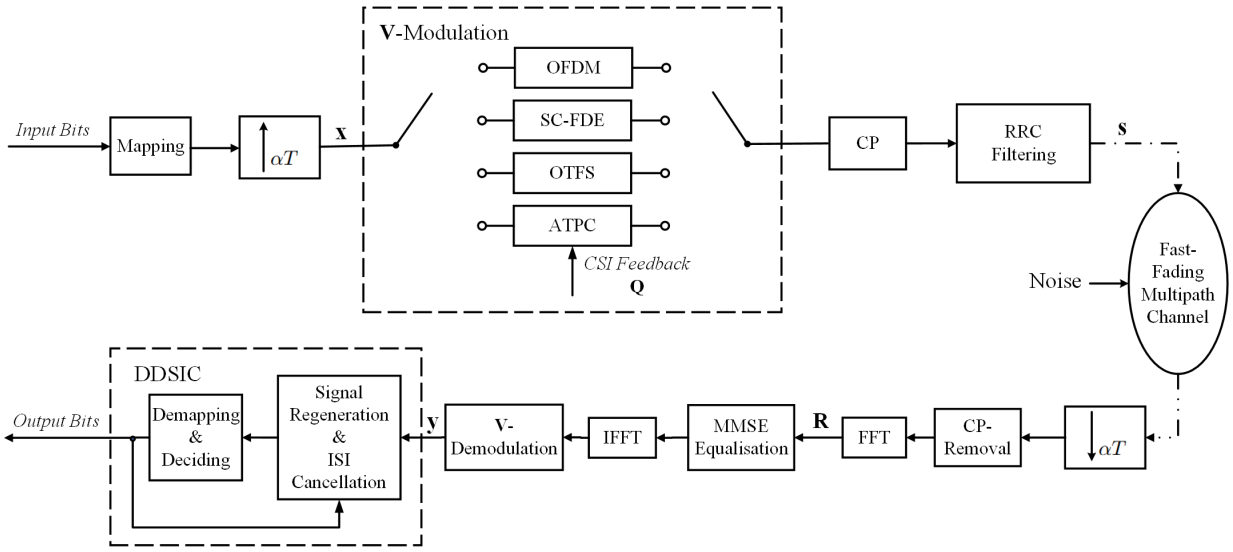

Fig. 1: Block diagram of the proposed FTN adaptive transmission system.

as $g(x) = \frac{\sin(\pi x)}{\pi x}$ if no windowing other than rectangular windowing is explicitly applied in the time domain, supporting both integral and fractional time delay and Doppler shifts, and P, is the number of fading channel impulse response (CIR) paths. The corresponding frequency-Doppler domain channel representation is defined as

$$H_\nu(f,\nu) = \int_{-\infty}^{+\infty} h(\tau,\nu) e^{-j2\pi f\tau} d\tau, \tag{3}$$

which is determined by h_i, τ_i and ν_i in such a sparse P-path channel. As the RRC filter is treated as part of the overall communication channel, the ISI caused by FTN signaling and by the propagation channel are jointly analyzed and mitigated in subsequent cancellation processes.

At the receiver side, the received signals are sampled at αT. After removing the CP, the received signals are transformed into the FD via FFT. The received discrete FD signal can be expressed as

$$\mathbf{R} = \mathbf{H}_\nu \mathbf{S} + \mathbf{W}. \tag{4}$$

In (4), we have

$$\mathbf{H}_\nu = \begin{pmatrix} H_\nu[0,0] & \cdots & H_\nu[0,MN-1] \\ H_\nu[1,0] & \cdots & H_\nu[1,MN-1] \\ \vdots & \ddots & \vdots \\ H_\nu[MN-1,0] & \cdots & H_\nu[MN-1,MN-1] \end{pmatrix}, \alpha T \tag{5}$$

where the element at the i-th row and j-th column is $H_\nu[i,j] = H_\nu(if_r, jf_r)$, with $f_r = 1/(MN\alpha T)$ being the frequency resolution, $\mathbf{S}$ is the FFT of $\mathbf{s}$, and $\mathbf{W}$ represents the zero-mean white Gaussian noise vector with a variance of σ_w^2 for each element. $\mathbf{H}_\nu$ has a stripe diagonal structure with a stripe width of $2K_{max}$+1 due to the Doppler frequency shifts in fast-fading multipath channels. Additionally, $\mathbf{H}_\nu$ is a general model that can be applied to both integer and fractional time delays and Doppler shifts. Since our solution is applicated to any arbitrary $\mathbf{H}_\nu$, it is effective for both integer and fractional delays and Doppler shifts. For FTN signaling, $\mathbf{H}_\nu$ is not a full rank matrix since the frequency response is 0 at the edges of the signal spectrum due to RRC pulse shaping. To avoid confusion, the entire bandwidth of $\frac{1}{\alpha T}$ is defined as the FTN signal bandwidth and the bandwidth of non-zero samples, i.e., $(1+\beta)\frac{1}{T}$, is defined as the actually occupied bandwidth (AOB). To avoid potential FD overlapping, the AOB should be less than the FTN signal bandwidth. Therefore, the relationship between α and β is given by $\beta \leqslant \frac{1}{\alpha} - 1$ [35].

Then the signals are equalized by MMSE equalization. After equalization, further processing relying on $\mathbf{Q^H}$ and IFFT are applied for recovering the FTN signals, followed by decision-directed successive interference cancellation (DDSIC) [35] to remove the ISI. In each DDSIC iteration, the demodulated data bits are used for regenerating the noiseless received data signal to estimate the residual ISI. The DDSIC algorithm is an ISI cancellation algorithm that performs cancellation simultaneously for a complete frame. The first iteration of DDSIC performs MMSE equalization to recover the transmitted symbols and to remove most of the ISI. In the following several iterations, the signals are regenerated in an environment assumed to be noise-free, and the difference between the actual received signal and the regenerated signal is regarded as the residual ISI plus noise and be added to the detected symbols for the next ISI-removal iteration. As it has been proven in [35], it is capable of efficiently mitigating the ISI in slow-fading multipath channels without Doppler frequency shift. However, significant Doppler frequency shifts are introduced in fast-fading channels, leading to rapidly varying channel response vs. time. To resolve this problem, we introduce ATPC by constructing ATPC matrices corresponding to the current channel conditions, as it will be detailed in Section III.C. This adaptive approach mitigates the Doppler effect and maintains robust communication in fast-fading scenarios by supporting DDSIC in fast-fading channels.

B. Modulation Techniques Combined with FTN Signaling

For comparison with the proposed ATPC, we also examine the feasibility of integrating FTN into three state-of-the-art non-ATPC techniques: OFDM, SC-FDE and OTFS. We aim for assessing their potential compatibility for transmission over fast-fading multipath channels, i.e., the capability to achieve time and/or frequency diversity. For illustration purposes, we set $\alpha = 0.8$, $M = 8$ and $N = 1$ or 4 to show both the TD and FD waveforms generated from each modulation for a single transmitted data symbol $\mathbf{x} = [0, 1, 0, 0, 0, 0, 0, 0]^T$ having unit power. The TD and FD waveforms are shown in Fig. 2, and the frequency response of the RRC filter with roll-off factor $\beta = 0.2$ is also illustrated in each FD waveform to show the system's bandwidth.

The first subplots of Fig. 2(a) and Fig. 2(b) respectively illustrate the TD and FD signals of OFDM integrated with FTN. Observe that, in one FTN symbol duration ($8\alpha T$), the OFDM signal is a superposition of sinusoidal waves, thus the time-variant channel affects the information recovery to a lesser extent, since a data symbol lasts for the whole OFDM symbol duration, i.e., OFDM exhibits superb time-diversity. However, in the FD, some of the subcarrier components are suppressed by the FTN pulse shaping, thus part of the data signal is filtered out. Furthermore, the frequency-selective fading may further degrade the subcarrier components, hence the symbol recovery is seriously impacted. Consequently, OFDM fails to achieve frequency diversity.

On the other hand, in the integrated FTN SC-FDE scheme, the data information is confined to a single carrier, spreading its signal power over the available bandwidth, as shown in the second subplots of Fig. 2(a) and Fig. 2(b), respectively. Transmitting in time-varying channels, a data symbol may be seriously impacted due to the channel fluctuations, thus SC-FDE fails in achieving time diversity. In the FD, frequency-selective fading affects the data recovery to a lesser extent, since the frequency components are spread across the entire spectrum, thus SC-FDE achieves frequency diversity.

OTFS is a promising solution for practical fast-fading channels due to its high reliability and diversity gain, which has a good potential to be combined with FTN transmission. However, there is no literature on applying OTFS in FTN systems. As illustrated in the third subplots of Fig. 2(a) and Fig. 2(b), respectively, in the TD, each data symbol is transmitted in N time slots. Due to this replication, FTN-OTFS symbols are resistant to time-varying propagation to a certain extent. In the FD, the bandwidth is divided into M sub-bands and the signal components are spread in all these sub-bands. Although the RRC filter for FTN transmission may suppress the signal components at the edges of the passband, data information is still retained in other FD sub-bands, thus FTN-OTFS symbols can be recovered at the receiver. Therefore, FTN signaling over OTFS does not compromise either time- or frequency-diversity.

When applying ATPC, which will be detailed in Section III, both OFDM and SC-FDE are converted into short-frame modulation schemes, thereby effectively addressing their respective weaknesses in terms of their frequency and time diversity. Moreover, the OTFS scheme is expected to benefit from ATPC by stabilizing CSIs, and hence, enhancing its overall performance.

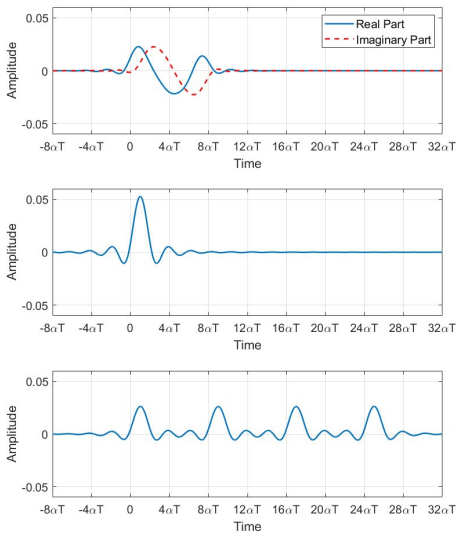

(a)

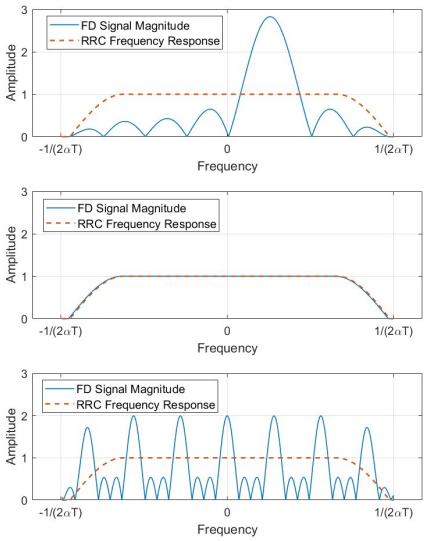

(b)

Fig. 2: Illustrations of modulated signal waveforms in (a) TD and (b) FD. The subplots from top to bottom represent OFDM ($M = 8, N = 1$), SC-FDE ($M = 8, N = 1$) and OTFS ($M = 8, N = 4$) schemes, respectively.

III. ATPC and Performance Analysis

In this section, we provide a more detailed description of the ATPC and analyze the BER performance of FTN signaling schemes under fast-fading multipath channels.

A. MMSE Equalization in Frequency Domain

Frequency-domain MMSE equalization is applied for mitigating the fast-fading multipath channel effect as the first step. Compared to TD equalizations, linear convolution and matrix inversion operations are simplified into multiplication or division operations, which efficiently reduces the computational complexity [35]. The matrix form of the MMSE equalization is defined as

$$\mathbf{E}_\nu = \mathbf{H}_\nu^{\mathbf{H}}(\mathbf{H}_\nu\mathbf{H}_\nu^{\mathbf{H}} + \frac{1}{\gamma_{in}}\mathbf{I}_{MN})^{-1}, \tag{6}$$

where $\{\cdot\}^{\mathbf{H}}$ denotes the conjugate transposition of a matrix, γ_{in} is the input SNR of MMSE equalizer, and $\mathbf{I}_{MN}$ is the identity matrix of order MN. It is highlighted that there are many zero samples in the RRC frequency response within the FTN signal bandwidth, hence conventional zero-forcing equalization fails to work.

The equalized FD signal can be formulated as

$$\hat{\mathbf{S}} = \mathbf{E}_\nu\mathbf{R} = \mathbf{E}_\nu\mathbf{H}_\nu\mathbf{S} + \mathbf{E}_\nu\mathbf{W}. \tag{7}$$

B. Demodulation and Output SNR

After equalization, demodulation is carried out by applying the matrix $\mathbf{V}^{\mathbf{H}}$ to remove the ISI and to recover the data symbols. It is assumed that modulation and demodulation can be regarded as reciprocal processes, i.e., the modulation matrix $\mathbf{V}$ and demodulation matrix $\mathbf{V}^{\mathbf{H}}$ satisfy $\mathbf{V}^{\mathbf{H}}\mathbf{V} = \mathbf{V}\mathbf{V}^{\mathbf{H}} = \mathbf{I}_{MN}$.

The demodulated signals are expressed as

$$\begin{aligned}\mathbf{y} &= \mathbf{V}^{\mathbf{H}}\mathbf{F}_{MN}^{\mathbf{H}}\hat{\mathbf{S}} \\ &= \mathbf{V}^{\mathbf{H}}\mathbf{F}_{MN}^{\mathbf{H}}\mathbf{E}_\nu\mathbf{H}_\nu\mathbf{F}_{MN}\mathbf{V}\mathbf{x} + \mathbf{V}^{\mathbf{H}}\mathbf{F}_{MN}^{\mathbf{H}}\mathbf{E}_\nu\mathbf{F}_{MN}\mathbf{w}.\end{aligned} \tag{8}$$

Since the fast-fading channel's matrix $\mathbf{H}_\nu$ is not a circular matrix, it cannot be directly decomposed as in [35]. Hence we harness the eigenvalue-based matrix decomposition of the Hermitian matrix $\mathbf{H}_\nu^{\mathbf{H}}\mathbf{H}_\nu$ formulated as

$$\mathbf{H}_\nu^{\mathbf{H}}\mathbf{H}_\nu = \mathbf{Q}\mathbf{\Psi}\mathbf{Q}^{\mathbf{H}}, \tag{9}$$

where $\mathbf{Q}$ is the feedback information to the transmitter. $\mathbf{Q}$ is a unitary matrix of $MN \times MN$, $\mathbf{Q}$ and $\mathbf{Q}^{\mathbf{H}}$ satisfy $\mathbf{Q}\mathbf{Q}^{\mathbf{H}} = \mathbf{I}_{MN}$, and $\mathbf{\Psi}$ is a diagonal matrix with λ_i being the i-th diagonal element. The elements on the diagonal are eigenvalues of the matrix $\mathbf{H}_\nu^{\mathbf{H}}\mathbf{H}_\nu$.

In (8), the equivalent transfer matrix from $\mathbf{x}$ to $\mathbf{y}$ can be defined as

$$\mathbf{P} = \mathbf{V}^{\mathbf{H}}\mathbf{F}_{MN}^{\mathbf{H}}\mathbf{E}_\nu\mathbf{H}_\nu\mathbf{F}_{MN}\mathbf{V}. \tag{10}$$

Upon defining

$$\mathbf{U} = \mathbf{V}^{\mathbf{H}}\mathbf{F}_{MN}^{\mathbf{H}}\mathbf{Q}, \tag{11}$$

$\mathbf{P}$ can be simplified as (see Appendix A)

$$\mathbf{P} = \mathbf{I}_{MN} - \mathbf{U}\text{diag}\left\{\frac{1}{\gamma_{in}\lambda_i + 1}\right\}\mathbf{U}^{\mathbf{H}}, \tag{12}$$

where $\text{diag}\{x_i\}$ denotes a diagonal matrix with x_i as the i-th diagonal element. Based on the MMSE principle, the normalized noise-plus-interference power for the j-th equalized data symbol y_j which is the j-th element in $\mathbf{y}$ can be expressed as

$$\begin{aligned}J_j &= 1 - \sum \mathbf{P}[j,j] \\ &= \sum_{i=0}^{MN-1}\frac{1}{\gamma_{in}\lambda_i + 1}|\mathbf{U}[j,i]|^2.\end{aligned} \tag{13}$$

The output SNR for the j-th symbol after MMSE equalization can be also derived as

$$\gamma_{out}[j] = \frac{1 - J_j}{J_j}. \tag{14}$$

Note that the output SNR is independent of the transmitted data symbol $\mathbf{x}[j]$ because the average power of the transmitted signal and shaping pulse are both normalized to 1. Additionally, the relationship between the output SNR and noise-plus-interference component is a general and normalized expression, which is also independent of the modulation scheme.

C. ATPC Method

The design of the ATPC scheme should meet two goals. Firstly, it may be inferred from (13) that the noise-plus-interference power is related to the matrix $\mathbf{U}$, which is further related to the modulation matrix $\mathbf{V}$ and eigenvector matrix $\mathbf{Q}$. Thus the ATPC scheme should be designed for minimizing the noise power and hence maximize the output SNR. Secondly, as discussed in Section II.A, this scheme should also be designed for mitigating the Doppler effect, i.e., establishing a slow-fading decomposed matrix form for DDSIC.

Therefore, we start from $\mathbf{U}$ and arrange for it to satisfy

$$\mathbf{U} = \mathbf{F}_{MN}^{\mathbf{H}}, \tag{15}$$

which minimizes the overall average BER (see Appendix B).

Once adaptive transmission is applied based on (12) and (15), $\mathbf{P}$ becomes

$$\begin{aligned}\mathbf{P} &= \mathbf{I}_{MN} - \mathbf{F}_{MN}^{\mathbf{H}}\text{diag}\left\{\frac{1}{\gamma_{in}\lambda_i + 1}\right\}\mathbf{F}_{MN} \\ &= \mathbf{F}_{MN}^{\mathbf{H}}\text{diag}\left\{\frac{\gamma_{in}\lambda_i}{\gamma_{in}\lambda_i + 1}\right\}\mathbf{F}_{MN},\end{aligned} \tag{16}$$

which is a circular matrix with the same diagonal elements.

Observe in (16) that $\mathbf{P}$ has a similar decomposed form as in slow-fading channels [35]. This means that, after incorporating the ATPC module in the FTN system, the Doppler effect will be mitigated. DDSIC can then be readily employed for removing the ISI.

Now the average noise-plus-interference power and the output SNR of all equalized data symbols are the same respectively, hence (13) and (14) become

$$J = \frac{1}{MN}\sum_{i=0}^{MN-1}\frac{1}{\gamma_{in}\lambda_i + 1} \tag{17}$$

and

$$\gamma_{out} = \frac{1 - J}{J} = \frac{1}{\frac{1}{MN}\sum_{i=0}^{MN-1}\frac{1}{\gamma_{in}\lambda_i + 1}} - 1. \tag{18}$$

According to (11) and (15), $\mathbf{V} = \mathbf{F}_{MN}^{\mathbf{H}}\mathbf{Q}\mathbf{F}_{MN}$ is no longer a conventional modulation matrix, which means that if $\mathbf{V}$ is chosen according to $\mathbf{Q}$, i.e., it is adaptive to the CSI fluctuations, the detection performance will be optimized. Therefore, we term this method ATPC. Note that the feedback matrix $\mathbf{Q}$ here is assumed to be constant. Although the CSI varies rapidly for all the OTFS schemes, MN samples are hosted by a coherent processing interval, during which the channel parameters can be assumed to be unchanged. The channel reciprocity and CSI robustness of rapidly fading time division duplex (TDD) systems still holds, according to [36].

D. Performance after DDSIC

In order to separate the ISI component from the received signals, we define $\mathbf{G} = \mathbf{V}^{\mathbf{H}}\mathbf{F}_{MN}^{\mathbf{H}}\mathbf{E}_{\nu}\mathbf{F}_{MN}$ and reformulate (8) as

$$\begin{aligned}\mathbf{y} &= \mathbf{P}\mathbf{x} + \mathbf{G}\mathbf{w} \\ &= p_0\mathbf{x} + (\mathbf{P} - p_0\mathbf{I}_{MN})\mathbf{x} + \mathbf{G}\mathbf{w},\end{aligned} \tag{19}$$

where p_0 is the diagonal element in $\mathbf{P}$, $\mathbf{w}$ is the TD noise vector before equalization, the term $p_0\mathbf{x}$ represents the desired signals, the second term is the ISI caused by FTN signaling and propagation channel and the last one is the noise after equalization.

It has been demonstrated that, after five iterations, the ISI can be almost completely eliminated [35]. Considering the optimal scenario that all the ISI is removed by DDSIC, in the presence of the noise component only, the output SNR can be derived as

$$\begin{aligned}\gamma_0 &= \frac{\text{Power}\left\{\text{desired signal}\right\}}{\text{Power}\left\{\text{noise}\right\}} \\ &= \frac{1}{MN}\frac{(\sum_{i=0}^{MN-1}\frac{\gamma_{in}\lambda_i}{\gamma_{in}\lambda_i+1})^2}{\sum_{i=0}^{MN-1}\frac{\gamma_{in}\lambda_i}{(\gamma_{in}\lambda_i+1)^2}}.\end{aligned} \tag{20}$$

The detailed derivation is provided in Appendix C.

Then the BER can be expressed as

$$\begin{aligned}P_b &\approx \frac{2(1-2^{-k})}{k}Q\left(\sqrt{\frac{3}{4^k-1}\gamma_0}\right) \\ &= \frac{2(1-2^{-k})}{k}Q\Bigg(\sqrt{\frac{3}{4^k-1}} \\ &\quad \sqrt{\frac{1}{MN}\frac{(\sum_{i=0}^{MN-1}\frac{\gamma_{in}\lambda_i}{\gamma_{in}\lambda_i+1})^2}{\sum_{i=0}^{MN-1}\frac{\gamma_{in}\lambda_i}{(\gamma_{in}\lambda_i+1)^2}}}\Bigg).\end{aligned} \tag{21}$$

where k is the modulation order (for 4-QAM, $k = 1$, and for 16-QAM, $k = 2$, etc.) while $Q(\cdot)$ is the Q-function defined as $Q(x) = \frac{1}{\sqrt{2\pi}}\int_x^{\infty} e^{-\frac{t^2}{2}}dt$.

IV. Performance Benchmarks in Extreme Conditions

In this section, we consider two extreme channel conditions and derive the corresponding BER expressions, which will be shown to be related to the number of CIR paths in the fast-fading channel, P, and the maximum number of positive resolvable Doppler frequencies $K_{max} = f_{max}/f_r$, where f_{max} is the maximum Doppler frequency shift.

A. Zero Eigenvalue Distribution Discussion

From (21), the BER performance of the adaptive FTN transmission is determined by the eigenvalues of the Hermitian matrix $\mathbf{H}_{\nu}^{\mathbf{H}}\mathbf{H}_{\nu}$, λ_i for $i = 0, 1, ..., MN-1$. For conventional transmission without FTN, $\mathbf{H}_{\nu}^{\mathbf{H}}\mathbf{H}_{\nu}$ is of full-rank and λ_i are all non-zero. However, for FTN, zero eigenvalues will be introduced. As shown in Fig. 2, FTN pulse shaping results in bandwidth reduction and in the emergence of zero samples at the edges of FTN signal bandwidth, carrying no information. As the symbol rate is increased to $1/\alpha T$, the number of these zero samples increases upon reducing β. As the RRC filter is considered to be part of the channel during our performance analysis, the zero samples can lead to the presence of zero eigenvalues in the channel decomposition. Hence, it becomes imperative to incorporate the increased number of zero-eigenvalues introduced by the RRC filter into the distribution of λ_i.

Based on the well-known eigenvalue probability density functions (PDFs) of a full-rank Hermitian matrix under the pair of extreme conditions considered, we now modify and reformulate the eigenvalue distribution by taking into account the time shrinkage factor α and roll-off factor β for FTN signaling.

As shown in Fig. 2 (b), non-zero samples, which can be represented by the conventional PDFs, occupy a fraction of $\alpha(1+\beta)$ in the FTN signal bandwidth, and the zero-samples, which have to be added in the conventional full-ranked eigenvalue PDFs, occupy a fraction of $1-\alpha(1+\beta)$ in the FTN signal bandwidth. Therefore, assuming that all the zero-eigenvalues caused by RRC filtering are represented by an impulse function as $MN \to \infty$ in the eigenvalue PDFs, and let $\eta = \alpha(1+\beta)$, the modified eigenvalue PDFs of FTN can be expressed as $\eta p_{\lambda}(\rho) + (1-\eta)\delta(\rho)$, where $p_{\lambda}(\cdot)$ denotes the conventional full-ranked eigenvalue PDFs, ρ denotes the eigenvalue variable and $\delta(\cdot)$ is the Dirac delta function.

To facilitate the follow-up evaluation, the expression of (20) is reformulated as

$$\gamma_0 = \frac{(1-\frac{1}{MN}\sum_{i=0}^{MN-1}\frac{1}{\gamma_{in}\lambda_i+1})^2}{\frac{1}{MN}\sum_{i=0}^{MN-1}\frac{1}{\gamma_{in}\lambda_i+1} - \frac{1}{MN}\sum_{i=0}^{MN-1}\frac{1}{(\gamma_{in}\lambda_i+1)^2}}. \tag{22}$$

B. Extreme Case One: Infinite-Multipath

The first extreme channel condition occurs when there is no Doppler frequency shift in any of the multipath components, but P is infinite. In this case, the signal transmission enjoys full frequency diversity, hence the BER approaches its lower bound. This is an extreme slow-fading condition.

Assuming that all the multipath components are independent, the FD channel matrix can be expressed as $\mathbf{H}_{\nu} = \text{diag}\{\psi_i\}$ with the fading gain ψ_i of each path obeying Gaussian distribution. Hence the eigenvalue $\lambda_i = |\psi_i|^2$ obeys chi-square distribution with two degrees of freedom and $p_{\lambda}(\rho) = e^{-\rho}$ [37]. For FTN transmission, the PDF is approximated as $\eta e^{-\rho} + (1-\eta)\delta(\rho)$. Therefore, the output

SNR for the ISI-decontaminated symbols under the adaptive transmission regime can be expressed for $MN \to \infty$ as

$$\begin{aligned}\gamma_{low} &= \frac{[1-\int_0^{\infty}\frac{\eta e^{-\rho}+(1-\eta)\delta(\rho)}{\gamma_{in}\rho+1}d\rho]^2}{\int_0^{\infty}\frac{\eta e^{-\rho}+(1-\eta)\delta(\rho)}{\gamma_{in}\rho+1}d\rho-\int_0^{\infty}\frac{\eta e^{-\rho}+(1-\eta)\delta(\rho)}{(\gamma_{in}\rho+1)^2}d\rho} \\ &= \frac{\eta\gamma_{in}(1-\frac{1}{\gamma_{in}}E_1(\frac{1}{\gamma_{in}})e^{\frac{1}{\gamma_{in}}})^2}{E_1(\frac{1}{\gamma_{in}})e^{\frac{1}{\gamma_{in}}}+\frac{1}{\gamma_{in}}E_1(\frac{1}{\gamma_{in}})-e^{-\frac{1}{\gamma_{in}}}},\end{aligned} \tag{23}$$

where $E_1(\cdot)$ is the first-order exponential integral function, which is defined as

$$E_1(z)=\int_z^{\infty}\frac{e^{-t}}{t}dt. \tag{24}$$

The BER lower bound is then given by

$$P_{b,low}=\frac{2(1-2^{-k})}{k}Q\left(\sqrt{\frac{3}{4^k-1}\sqrt{\frac{\eta\gamma_{in}(1-\frac{1}{\gamma_{in}}E_1(\frac{1}{\gamma_{in}})e^{\frac{1}{\gamma_{in}}})^2}{E_1(\frac{1}{\gamma_{in}})e^{\frac{1}{\gamma_{in}}}+\frac{1}{\gamma_{in}}E_1(\frac{1}{\gamma_{in}})-e^{-\frac{1}{\gamma_{in}}}}}}\right). \tag{25}$$

C. Extreme Case Two: Infinite-Doppler

The second extreme scenario is that of an infinite value of K_{max}. Assuming that the Doppler frequencies are uniformly distributed and the number of paths is as large as possible, every element in $\mathbf{H}_\nu$ is a Gaussian random variable. In this case, the time diversity order is maximal. Then $\mathbf{H}_\nu^{\mathbf{H}}\mathbf{H}_\nu$ obeys Wishart distribution and $p_\lambda(\rho)=\frac{1}{2\pi}\sqrt{\frac{4-\rho}{\rho}}, 0\leqslant\rho\leqslant 4$ [38], if $\mathbf{H}_\nu$ is full ranked without FTN. For FTN transmission, the PDF is approximated as $\eta\frac{1}{2\pi}\sqrt{\frac{4-\rho}{\rho}}+(1-\eta)\delta(\rho)$. Therefore, the output SNR for the ISI-free symbol under the adaptive transmission regime can be formulated for $MN\to\infty$, as

$$\begin{aligned}\gamma_{up} &= \frac{[1-\int_0^4\frac{\frac{1}{2\pi}\sqrt{\frac{4-\rho}{\rho}}\eta+(1-\eta)\delta(\rho)}{\gamma_{in}\rho+1}d\rho]^2}{\int_0^4\frac{\frac{1}{2\pi}\sqrt{\frac{4-\rho}{\rho}}\eta+(1-\eta)\delta(\rho)}{\gamma_{in}\rho+1}d\rho-\int_0^4\frac{\frac{1}{2\pi}\sqrt{\frac{4-\rho}{\rho}}\eta+(1-\eta)\delta(\rho)}{(\gamma_{in}\rho+1)^2}d\rho} \\ &= \frac{\eta(1-\frac{\sqrt{4\gamma_{in}+1}-1}{2\gamma_{in}})^2}{\frac{\sqrt{4\gamma_{in}+1}-1}{2\gamma_{in}}-\frac{1}{\sqrt{4\gamma_{in}+1}}}.\end{aligned} \tag{26}$$

Therefore, the infinite-Doppler BER expression is given by

$$P_{b,up}=\frac{2(1-2^{-k})}{k}Q\left(\sqrt{\frac{3}{4^k-1}\frac{\eta(1-\frac{\sqrt{4\gamma_{in}+1}-1}{2\gamma_{in}})^2}{\frac{\sqrt{4\gamma_{in}+1}-1}{2\gamma_{in}}-\frac{1}{\sqrt{4\gamma_{in}+1}}}}\right). \tag{27}$$

V. Simulation Results

In this section, we consider the BER and evaluate the performance of our proposed adaptive FTN transmission system in different channel conditions. The system parameters are listed in Table II. It has been discussed in Section III.C that, after ATPC, the modulation matrix $\mathbf{V}$ is only related to the CSI, M and N. Therefore, after ATPC, the OFDM and SC-FDE modulations are regarded as the same and again, they are referred to as a short-frame adaptive scheme with a frame length of M plus the CP. Similarly, OTFS after ATPC is regarded as a long-frame adaptive scheme with a frame length of MN plus the CP. In order to explore the feasibility of combining the three modulation methods with FTN signaling, the BER performances of OFDM-FTN, SC-FDE-FTN and OTFS-FTN are compared by adopting both QPSK and 16-QAM. Without loss of generality, both LOS and NLOS multipath fading channels are considered for evaluating the BER performance. The LOS and NLOS channel models are tapped delay line (TDL) channel models along with multipath time delay, which are introduced in the European Telecommunications Standards Institute (ETSI) recommendation and have been broadly employed to represent realistic circumstances [39]. The remaining fading channel parameters of the TDL-A and TDL-D channel models are listed in Table III.

TABLE II: SIMULATION PARAMETERS I

No. of Subcarriers (M)	256	No. of Symbols in Each Subcarrier (N)	32
Time Acceleration Factor (α)	0.8	Roll-off Factor of RRC Filter (β)	0.2
Carrier Frequency (f_c)	6 GHz	Subcarrier Spacing (Δf)	6.144 MHz
Nyquist Bandwidth ($W=\alpha M\Delta f$)	30 kHz	Nyquist Symbol Duration ($T=1/W$)	162.76 ns
Delay Resolution ($d_r=\alpha T$)	162.76 ns	Doppler Resolution ($f_r=1/(MN\alpha T)$)	750.002 Hz
Bandwidth of FTN Symbols ($B=(1+\beta)/T$))	7.37 MHz		

A. Resistance of ATPC to Doppler Effect

In order to verify whether ATPC is capable of creating a relatively Doppler-free environment for further ISI cancellation, we first assume that each path shares the same power, and maintain $P=M$ to ensure full multipath diversity, while changing the value of K_{max} to observe the BER performance of long-adaptive transmission (including MN data symbols in each frame) under the fast fading channel.

TABLE III: SIMULATION PARAMETERS II

Maximum Speed (v_{max})	500 km/h	Maximum Doppler Frequency ($f_{max}=f_c\frac{v_{max}}{v_c}$, $v_c=3\times10^8$m/s)	2777.8 Hz
No. of Doppler Shifts (Positive or Negative) ($K_{max}=\lceil\frac{f_{max}}{f_r}\rceil$)	≈ 3	Maximum Delay (d_{max})	3820.6 ns (LOS), 3506.1 ns (NLOS)
No. of Multipaths ($L_{max}=\lceil\frac{d_{max}}{d_r}\rceil$)	29 (LOS), 27 (NLOS)		

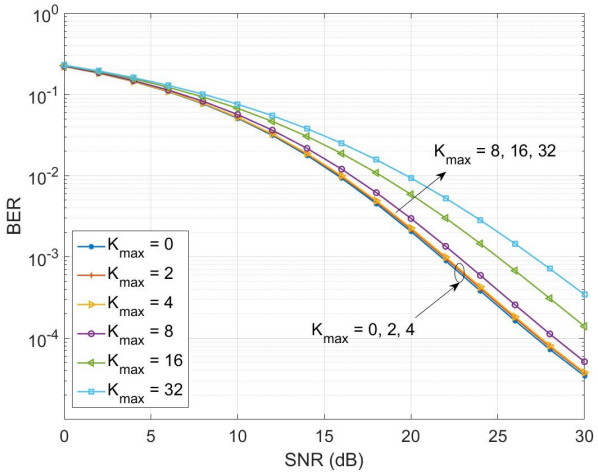

Fig. 3: BER comparison between adaptive transmission (without DDSIC), with different maximum Doppler frequency shifts with QPSK modulation under multipath Rayleigh fast-fading channel.

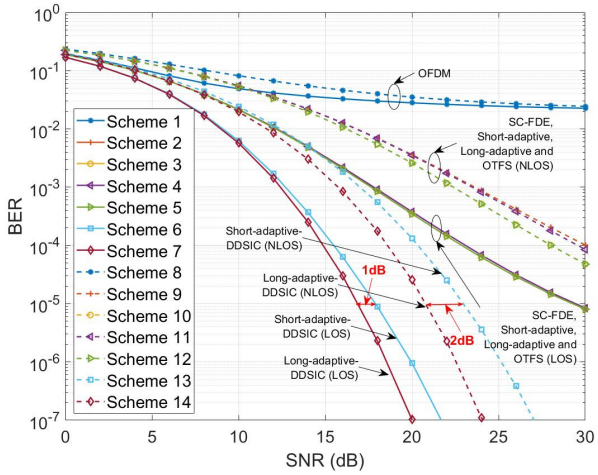

Fig. 4: BER comparison between different modulation schemes with QPSK modulation under LOS and NLOS channels.

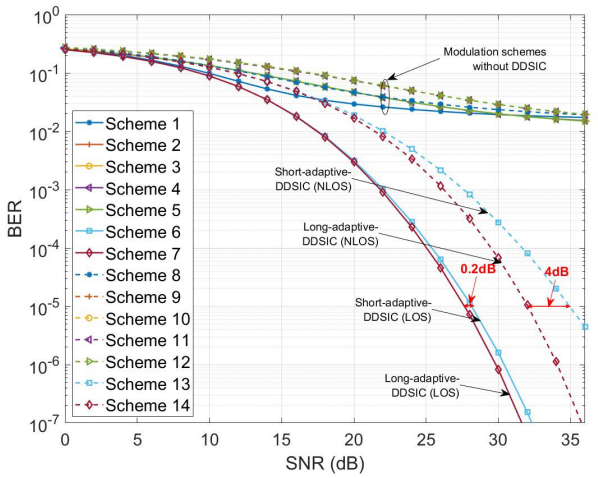

Fig. 5: BER comparison between different modulation schemes with 16-QAM modulation under LOS and NLOS channels.

Fig. 3 shows that, when K_{max} is under a threshold of 8, the BERs of FTN adaptive transmission without DDSIC are nearly the same, which demonstrates that the ATPC efficiently mitigates the Doppler effect. Note that this threshold K_{max} is jointly related to v_{max}, f_c, M, N, T, α and the channel factors, including the number of delay taps, delay value and power of each tap. Adopting QPSK, when $K_{max} < 8$, where the maximum vehicular speed is 1350 km/h, the Doppler effect is totally eliminated, which represents an aircraft scenario. Additionally, when K_{max} exceeds this threshold, ATPC fails to completely remove the Doppler effect and hence there is a degradation, which is still an acceptable difference that allows the application of DDSIC.

B. BER Performance Comparison after DDSIC

All the simulated modulation schemes are described in Table IV, and the BER comparisons are shown in Figs. 4 and 5. Observe in these two figures that the proposed ATPC-aided DDSIC scheme shows a satisfactory performance under both LOS and NLOS channels and for both QPSK and 16-QAM mappings. Since the time-selectivity is relatively modest, whereas the frequency-selectivity is prominent in the channels considered, the impact of time variability is low compared to the significant effects of frequency selectivity. Therefore, the OFDM-FTN scheme fails to achieve full diversity and exhibits an eroded performance in every condition. the OFDM-FTN scheme fails to achieve full diversity and exhibits an eroded performance in every condition. Adopting QPSK modulation and a target BER of 10^{-5}, the ATPC exhibits a 12 dB gain, when DDSIC is employed. Notably, long-frame transmission results in better performance than short-frame transmission. For the target BER of 10^{-5}, there is a 1 dB gap between the two transmission schemes under LOS channels and a 2 dB gap under NLOS channels. Upon adopting 16-QAM, the ISI has such a grave impact on the system performance, thus the schemes without interference cancellation do not work. However, ATPC-aided DDSIC still works well and for the target BER of 10^{-5}, there is only a 0.2 dB gap between the long and short-frame adaptive transmission schemes under LOS channels and a 4 dB gap under NLOS channels.

In order to study the robustness of the proposed adaptive-DDSIC scheme to various Doppler frequencies, the simulated BERs of the scheme under different v_{max} values and the TDL-D channel are illustrated in Fig. 6, where the input SNRs are set as 17 dB and QPSK modulation is adopted. Observe that upon increasing v_{max}, the BER only fluctuates within a small range, which demonstrates that the proposed TPC-DDSIC scheme is robust to a wide range of Doppler frequencies.

Considering practical transmission associated with imperfect channel states, the BER performance comparison of an

TABLE IV: MODULATION SCHEME DESCRIPTION

No.	Modulation Scheme	Frame Length (Short for $M = 256, N = 1$ and Long for $M = 256$, $N = 32$)	Channel Type	Combined with ATPC	Combined with DDSIC
1	OFDM	Short	LOS	✘	✘
2	SC-FDE	Short	LOS	✘	✘
3	OTFS	Long	LOS	✘	✘
4	OFDM/SC-FDE-adaptive	Short	LOS	✔	✘
5	OTFS-adaptive	Long	LOS	✔	✘
6	OFDM/SC-FDE-adaptive-DDSIC	Short	LOS	✔	✔
7	OTFS-adaptive-DDSIC	Long	LOS	✔	✔
8	OFDM	Short	NLOS	✘	✘
9	SC-FDE	Short	NLOS	✘	✘
10	OTFS	Long	NLOS	✘	✘
11	OFDM/SC-FDE-adaptive	Short	NLOS	✔	✘
12	OTFS-adaptive	Long	NLOS	✔	✘
13	OFDM/SC-FDE-adaptive-DDSIC	Short	NLOS	✔	✔
14	OTFS-adaptive-DDSIC	Long	NLOS	✔	✔

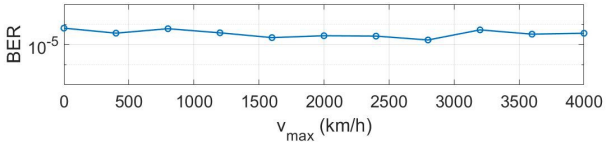

Fig. 6: BER performance at different maximum speeds for SNR = 17 dB under LOS channel with QPSK modulation.

ideal and two practical long-frame transmission scenarios is illustrated in Fig. 7. The first scenario considers fractional time delays and Doppler shifts, and the second considers channel estimation errors simulated by introducing zero-mean random additive Gaussian noise with a variance of $\frac{1}{2\gamma_{in}}$, resulting in imperfect CSI (ICSI) feedback. The simulation results demonstrate that the proposed scheme is robust to both practical scenarios. In the first scenario, for the target BER of 10^{-5}, the gaps between fractional delay-Doppler and perfect transmission are only 1 dB under LOS channels and 0.5 dB under NLOS channels. Regarding the second scenario, for the target BER of 10^{-5}, the gaps between ICSI feedback and perfect transmission are only 1.5 dB under LOS channels and 1 dB under NLOS channels.

C. Extreme Case Benchmarks

Since the DDSIC algorithm is seen to be able to efficiently remove the ISI under both LOS and NLOS channels, we further compare the BER performances in two extreme cases, as discussed in Section IV. To ensure that all paths are independent and of equal power, Rayleigh fading channels are employed, and the Doppler frequency shifts are assumed to be static and uniformly distributed from $-K_{max}$ to K_{max}. In the first extreme case, we keep K_{max} as 0 and increase P. Then the theoretical BER curves are compared against the lower bound derived.

Fig. 8 indicates that, as the number of paths approaches the number of subcarriers, M, the curves approach the lower bound derived. Due to the eigenvalue PDF approximation, there is a gap of about 2 dB between the lower bound derived and the theoretical BER curve for $P = M$ at the target BER of 10^{-5}, which is an acceptable difference.

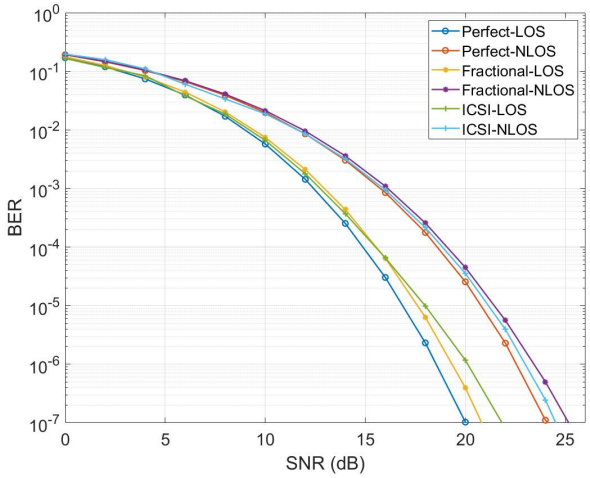

Fig. 7: BER comparison between perfect and imperfect transmission scenarios with QPSK modulation under LOS and NLOS channels.

In the second extreme case, to verify the BER trend associated with the maximum diversity order of our proposed system, we keep $P = M$ to ensure full multipath diversity and increase K_{max} gradually. In this case, the slopes of the BER curves are observed, which represent the diversity order when the SNR increases towards infinity. As P is fixed to M, all elements in the channel matrix are independent and random. The various BER curves recorded for different K_{max} and the infinite-Doppler BER curve derived for the low SNR region are illustrated in Fig. 9. As it is mentioned in Section V.A, under the threshold of $K_{max} = 8$, the Doppler effects can be totally eliminated by ATPC. In this case, our infinite-Doppler curve characterizes the upper bound of the BER performance. In the high SNR region, we observe from Fig. 10 that the slope of the infinite-Doppler curve becomes the steepest among all BER curves. This is close to the theoretical BER curve for $K_{max} = 32$. Generally, we can conclude that the larger the K_{max}, the higher the diversity order. However, note that the results for $K_{max} = 1$ in Fig. 10 are special, because the slope has not stabilized as the SNR region selected has not been extended to infinity. Additional simulation results disclose that

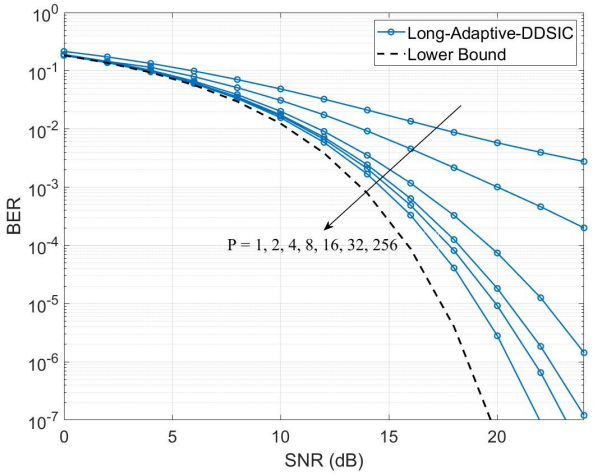

Fig. 8: Derived lower bound and BER performance of ATPC-aided DDSIC adopting different multipath numbers under multipath Rayleigh fast-fading channels. The curves from right to left correspond to $P = 1, 2, 4, 8, 16, 32, 256$.

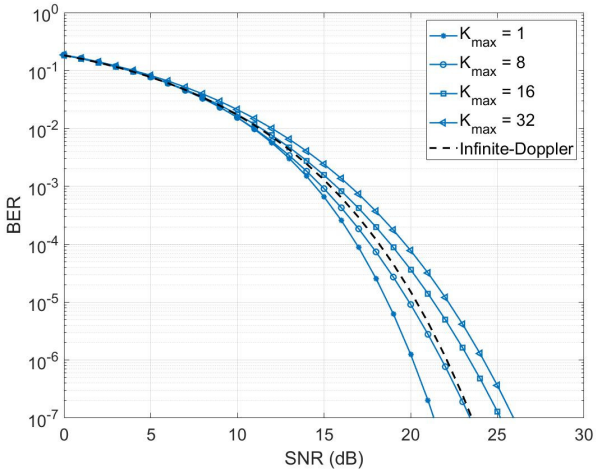

Fig. 9: BER comparison between derived infinite-Doppler curve and theoretical curves under multipath Rayleigh fast-fading channel employing different maximum Doppler frequencies with $P = M$.

when the SNR approaches infinity, the curve corresponding to $K_{max} = 1$ does not exhibit a steeper slope compared to the other curves. Consequently, the infinite-Doppler BER curve derived enjoys the highest diversity order, which demonstrates the accuracy of our infinite-Doppler BER expression derived.

D. Comparison among various Interference Cancellation Schemes and Combination with Channel Coding

In addition to the theoretical BER curves, we also quantified the BER performances of the FTN scenario and of the OTFS modulation scheme to explore the benefits of ATPC in the content of the BCJR-turbo detector and the truncated Viterbi (VA) detector. Moreover, low-density parity check (LDPC) channel coding is added to the proposed ATPC-aided DDSIC

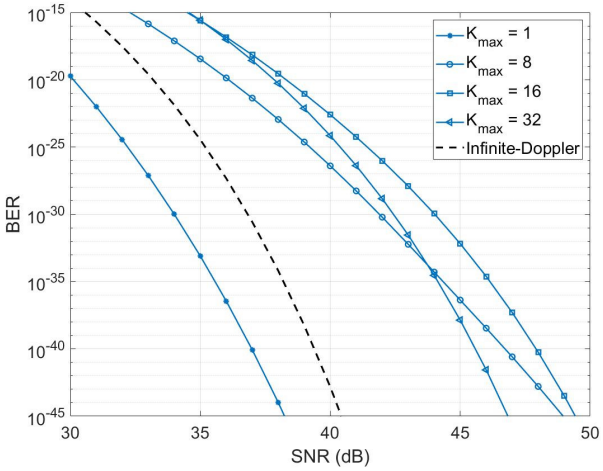

Fig. 10: BER comparison between derived infinite-Doppler curve and theoretical curves under multipath Rayleigh fast-fading channel employing different maximum Doppler frequencies in high SNR region.

algorithm and the BER is evaluated. In this simulation, the truncated ISI length of the truncated VA is set to 4, and the code rate of turbo and LDPC are both 0.75. The BER comparisons under TDL-D LOS and TDL-A NLOS channel models are illustrated in Figs. 11 and 12, respectively. Observe that under the LOS channel, the conventional DDSIC scheme operating without ATPC falters. Furthermore, ATPC-aided DDSIC has consistently lower BER than the truncated VA beyond the SNR of 8 dB. The BCJR detector with turbo coding exhibits good potential along with ATPC in the low SNR region but encounters an error floor beyond the SNR of 16 dB due to the limitation of turbo coding. Furthermore, the LDPC-coded scheme outperforms the ATPC-aided DDSIC scheme without coding by about 6 dB at the target BER of 10^{-4} and outperforms the ATPC-aided BCJR scheme beyond the SNR of 16 dB. Under the NLOS channel, the conventional DDSIC scheme falters and the truncated VA with ATPC performs poorly, whereas the proposed ATPC-aided DDSIC scheme and the ATPC-aided BCJR scheme still work well. Nonetheless, the ATPC-aided BCJR scheme encounters an error floor beyond an SNR of 15 dB, stabilizing at a BER of 9×10^{-5}. In contrast, the ATPC-aided DDSIC scheme with LDPC coding outperforms the ATPC-aided BCJR scheme above an SNR of 16 dB. Additionally, the LDPC-coded scheme outperforms the ATPC-aided DDSIC scheme without coding by approximately 4.8 dB at the target BER of 5×10^{-4}.

E. Discussion

The simulation results presented in this section demonstrate that the proposed ATPC method substantially mitigate the Doppler effect, allowing the DDSIC algorithm to be subsequently applied to further mitigate the ISI. Our extensive BER performance comparisons show that ATPC-aided modulation schemes can improve the diversity performance under both NLOS and LOS channels, as exemplified by both QPSK and

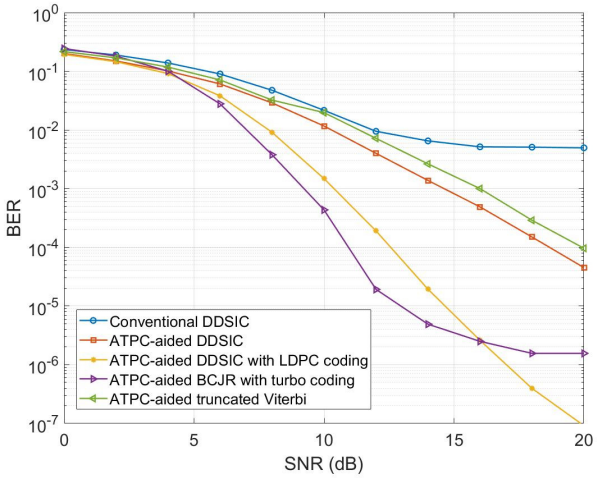

Fig. 11: BER performance of various interference cancellation schemes with QPSK modulation under LOS channel.

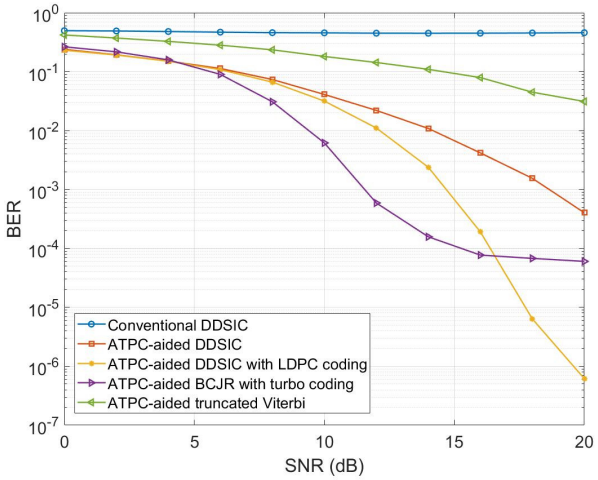

Fig. 12: BER performance of various interference cancellation schemes with QPSK modulation under NLOS channel.

16-QAM modulation, outperforming those operating without applying ATPC. Additionally, the DDSIC algorithm significantly enhances the BER performance for both channel types. The two closed-form theoretical bounds for the diversity performance are also validated.

VI. Conclusions

Adaptive FTN signaling has been proposed for rapidly-fading multipath channels. The modulation matrix used for ATPC can be determined by frequency-domain channel matrix eigenvalue decomposition and fed back to the transmitter. This new ATPC is capable of mitigating the Doppler effects so that a fast-fading channel multipath can be converted to a slow-fading one. The DDSIC conceived is therefore eminently suitable for mitigating the ISI caused by FTN and multipath. The BER performance after MMSE equalization and DDSIC is also analyzed. The closed-form BER expressions developed under two extreme channel conditions also provide useful theoretical performance benchmarks for FTN signaling under fast-fading multipath channels. Simulation results demonstrate the practical application feasibility of the proposed adaptive FTN scheme. The technique presented in this paper may be improved in several aspects. An important one is how to adopt codebook-based feedback instead of the $\mathbf{Q}$ matrix to significantly reduce the feedback overhead.

Acknowledgment

L. Hanzo would like to acknowledge the financial support of the Engineering and Physical Sciences Research Council (EPSRC) projects under grant EP/Y037243/1, EP/W016605/1, EP/X01228X/1, EP/Y026721/1, EP/W032635/1, EP/Y037243/1 and EP/X04047X/1 as well as of the European Research Council's Advanced Fellow Grant QuantCom (Grant No. 789028).

Appendix A

Based on (6) and (10), $\mathbf{P}$ can be further expanded as

$$\begin{aligned}\mathbf{P} &= \mathbf{V}^{\mathbf{H}}\mathbf{F}_{MN}^{\mathbf{H}}\mathbf{E}_{\nu}\mathbf{H}_{\nu}\mathbf{F}_{MN}\mathbf{V} \\ &= \mathbf{V}^{\mathbf{H}}\mathbf{F}_{MN}^{\mathbf{H}}\mathbf{H}_{\nu}^{\mathbf{H}}(\mathbf{H}_{\nu}\mathbf{H}_{\nu}^{\mathbf{H}}+\frac{1}{\gamma_{in}}\mathbf{I}_{MN})^{-1}\mathbf{H}_{\nu}\mathbf{F}_{MN}\mathbf{V} \\ &= (\mathbf{I}_{MN}+\frac{1}{\gamma_{in}}(\mathbf{V}^{\mathbf{H}}\mathbf{F}_{MN}^{\mathbf{H}}\mathbf{H}_{\nu}^{\mathbf{H}}\mathbf{H}_{\nu}\mathbf{F}_{MN}\mathbf{V})^{-1})^{-1}.\end{aligned} \tag{28}$$

Since $\mathbf{U}=\mathbf{V}^{\mathbf{H}}\mathbf{F}_{MN}^{\mathbf{H}}\mathbf{Q}$, this equation can be simplified as

$$\begin{aligned}\mathbf{P} &= (\mathbf{I}_{MN}+\frac{1}{\gamma_{in}}\mathbf{U}\mathbf{\Psi}^{-1}\mathbf{U}^{\mathbf{H}})^{-1} \\ &= \mathbf{I}_{MN}-\mathbf{U}\mathrm{diag}\left\{\frac{1}{\gamma_{in}\lambda_i+1}\right\}\mathbf{U}^{\mathbf{H}}.\end{aligned} \tag{29}$$

Appendix B

Jensen's inequality states that the convex transformation of a mean is always less than or equal to the mean applied after convex transformation [40], and the equality holds when the variable is constant in this transformation.

Since the BER for the symbol decided on the j-th element of $\mathbf{y}$ is determined based on a convex transformation of J_j through the SNR $\gamma_{out}[j]$ and a $Q(\cdot)$ function [41], the average BER for all symbols can be considered as the mean applied after convex transformation. According to Jensen's inequality, the average BER is minimized when all J_j are the same and equal to the mean of J_j. From (13), the average value of J_j can be expressed as

$$\begin{aligned}J &= 1-\frac{1}{MN}\mathrm{Tr}\{\mathbf{P}\} \\ &= \frac{1}{MN}\sum_{i=0}^{MN-1}\frac{1}{\gamma_{in}\lambda_i+1}.\end{aligned} \tag{30}$$

Hence, when $|\mathbf{U}[j,i]|^2=1$, all J_j are the same and equal to J. Then the average BER is minimized. Since $\mathbf{U}$ is an orthogonal matrix, it can be set as the IFFT matrix, i.e., $\mathbf{U}=\mathbf{F}_{MN}^{\mathbf{H}}$.

APPENDIX C

From (16), the weighting coefficient p_0 can be expressed as

$$p_0 = \frac{1}{MN}\mathrm{Tr}\{\mathbf{P}\} = \frac{1}{MN}\sum_{i=0}^{MN-1}\frac{\gamma_{in}\lambda_i}{\gamma_{in}\lambda_i+1}, \tag{31}$$

where $\mathrm{Tr}\{\cdot\}$ denotes the trace of a matrix.

In order to derive the power of the recovered signal, we first derive $\mathbf{PP^H}$ from (16) as

$$\mathbf{PP^H} = \mathbf{F}_{MN}^{\mathbf{H}}\mathrm{diag}\left\{(\frac{\gamma_{in}\lambda_i}{\gamma_{in}\lambda_i+1})^2\right\}\mathbf{F}_{MN}. \tag{32}$$

Upon defining $\mathbb{E}[\cdot]$ as the ensemble expectation, the covariance matrix of $\mathbf{y}$ is expressed as

$$\begin{aligned}
\mathbb{E}[\mathbf{yy^H}] &= \mathbb{E}[(\mathbf{Px}+\mathbf{Gw})(\mathbf{Px}+\mathbf{Gw})^{\mathbf{H}}] \\
&= \mathbf{P}\mathbb{E}[\mathbf{xx^H}]\mathbf{P^H} + \mathbf{G}\mathbb{E}[\mathbf{ww^H}]\mathbf{G^H} \\
&= \sigma_s^2\mathbf{PP^H} + \sigma_w^2\mathbf{GG^H} \\
&= \sigma_s^2(\mathbf{PP^H} + \frac{1}{\gamma_{in}}\mathbf{GG^H}) \\
&= \sigma_s^2(\mathbf{V^H}\mathbf{F}_{MN}^{\mathbf{H}}\mathbf{E}_\nu\mathbf{H}_\nu\mathbf{H}_\nu^{\mathbf{H}}\mathbf{E}_\nu^{\mathbf{H}}\mathbf{F}_{MN}\mathbf{V} + \\
&\frac{1}{\gamma_{in}}\mathbf{V^H}\mathbf{F}_{MN}^{\mathbf{H}}\mathbf{E}_\nu\mathbf{E}_\nu^{\mathbf{H}}\mathbf{F}_{MN}\mathbf{V}) \\
&= \sigma_s^2\mathbf{V^H}\mathbf{F}_{MN}^{\mathbf{H}}\mathbf{E}_\nu(\mathbf{H}_\nu\mathbf{H}_\nu^{\mathbf{H}} + \frac{1}{\gamma_{in}}\mathbf{I}_{MN})\mathbf{E}_\nu^{\mathbf{H}}\mathbf{F}_{MN}\mathbf{V} \\
&= \sigma_s^2\mathbf{V^H}\mathbf{F}_{MN}^{\mathbf{H}}\mathbf{E}_\nu^{\mathbf{H}}\mathbf{H}_\nu^{\mathbf{H}}\mathbf{F}_{MN}\mathbf{V} \\
&= \sigma_s^2\mathbf{P^H}.
\end{aligned} \tag{33}$$

Therefore, we can obtain the expression of (20) as

$$\begin{aligned}
\gamma_0 &= \frac{\text{Power}\{\text{desired signal}\}}{\text{Power}\{\text{noise}\}} \\
&= \frac{\frac{1}{MN}\mathrm{Tr}\left\{\mathbb{E}[p_0\mathbf{x}(p_0\mathbf{x})^{\mathbf{H}}]\right\}}{\frac{1}{MN}\mathrm{Tr}\{\mathbb{E}[\mathbf{yy^H}]\} - \frac{1}{MN}\mathrm{Tr}\{\mathbb{E}[\mathbf{Px}(\mathbf{Px})^{\mathbf{H}}]\}} \\
&= \frac{\sigma_s^2|p_0|^2}{\frac{1}{MN}\mathrm{Tr}\{\sigma_s^2\mathbf{P^H}\} - \frac{1}{MN}\mathrm{Tr}\{\sigma_s^2\mathbf{PP^H}\}} \\
&= \frac{1}{MN}\frac{(\sum_{i=0}^{MN-1}\frac{\gamma_{in}\lambda_i}{\gamma_{in}\lambda_i+1})^2}{\sum_{i=0}^{MN-1}\frac{\gamma_{in}\lambda_i}{\gamma_{in}\lambda_i+1} - \sum_{i=0}^{MN-1}(\frac{\gamma_{in}\lambda_i}{\gamma_{in}\lambda_i+1})^2} \\
&= \frac{1}{MN}\frac{(\sum_{i=0}^{MN-1}\frac{\gamma_{in}\lambda_i}{\gamma_{in}\lambda_i+1})^2}{\sum_{i=0}^{MN-1}\frac{\gamma_{in}\lambda_i}{(\gamma_{in}\lambda_i+1)^2}}.
\end{aligned} \tag{34}$$

REFERENCES

[1] J. B. Anderson, F. Rusek, and V. Öwall, "Faster-than-Nyquist signaling," *Proceedings of the IEEE*, vol. 101, no. 8, pp. 1817–1830, 2013.

[2] A. Ibrahim, E. Bedeer, and H. Yanikomeroglu, "A novel low complexity faster-than-Nyquist (FTN) signaling detector for ultra high-order QAM," *IEEE Open Journal of the Communications Society*, vol. 2, pp. 2566–2580, 2021.

[3] S. An, J. Li, X. Li, and Y. Su, "FTN SSB 16-QAM signal transmission and direct detection based on Tomlinson-Harashima precoding with computed coefficients," *Journal of Lightwave Technology*, vol. 39, no. 7, pp. 2059–2066, 2021.

[4] M. Ganji, X. Zou, and H. Jafarkhani, "On the capacity of faster than Nyquist signaling," *IEEE Communications Letters*, vol. 24, no. 6, pp. 1197–1201, 2020.

[5] F. Rusek and J. B. Anderson, "Constrained capacities for faster-than-Nyquist signaling," *IEEE Transactions on Information Theory*, vol. 55, no. 2, pp. 764–775, 2009.

[6] S. Li, B. Bai, J. Zhou, P. Chen, and Z. Yu, "Reduced-complexity equalization for faster-than-Nyquist signaling: New methods based on Ungerboeck observation model," *IEEE Transactions on Communications*, vol. 66, no. 3, pp. 1190–1204, 2017.

[7] M. J. L. Morales, D. Roque, and M. Benammar, "Timing estimation based on higher order cyclostationarity for faster-than-Nyquist signals," *IEEE Communications Letters*, vol. 23, no. 8, pp. 1373–1376, 2019.

[8] E. Bedeer, M. H. Ahmed, and H. Yanikomeroglu, "A very low complexity successive symbol-by-symbol sequence estimator for faster-than-Nyquist signaling," *IEEE Access*, vol. 5, pp. 7414–7422, 2017.

[9] S. Li, W. Yuan, J. Yuan, B. Bai, D. Wing Kwan Ng, and L. Hanzo, "Time-domain vs. frequency-domain equalization for FTN signaling," *IEEE Transactions on Vehicular Technology*, vol. 69, no. 8, pp. 9174–9179, 2020.

[10] A. Tajer and A. Nosratinia, "Diversity order in ISI channels with single-carrier frequency-domain equalizers," *IEEE Transactions on Wireless Communications*, vol. 9, no. 3, pp. 1022–1032, 2010.

[11] S. Wen, G. Liu, F. Xu, L. Zhang, C. Liu, and M. A. Imran, "Ergodic capacity of MIMO faster-than-Nyquist transmission over triply-selective Rayleigh fading channels," *IEEE Transactions on Communications*, vol. 70, no. 8, pp. 5046–5058, 2022.

[12] Z. Zhang, M. Yuksel, and H. Yanikomeroglu, "Faster-than-Nyquist signaling for MIMO communications," *IEEE Transactions on Wireless Communications*, vol. 22, no. 4, pp. 2379–2392, 2023.

[13] W. Yuan, N. Wu, A. Zhang, X. Huang, Y. Li, and L. Hanzo, "Iterative receiver design for FTN signaling aided sparse code multiple access," *IEEE Transactions on Wireless Communications*, vol. 19, no. 2, pp. 915–928, 2020.

[14] W. Yuan, N. Wu, Q. Guo, D. W. K. Ng, J. Yuan, and L. Hanzo, "Iterative joint channel estimation, user activity tracking, and data detection for FTN-NOMA systems supporting random access," *IEEE Transactions on Communications*, vol. 68, no. 5, pp. 2963–2977, 2020.

[15] T. Xu and I. Darwazeh, "A soft detector for spectrally efficient systems with non-orthogonal overlapped sub-carriers," *IEEE Communications Letters*, vol. 18, no. 10, pp. 1847–1850, 2014.

[16] Q. Shi, N. Wu, X. Ma, and H. Wang, "Frequency-domain joint channel estimation and decoding for faster-than-Nyquist signaling," *IEEE Transactions on Communications*, vol. 66, no. 2, pp. 781–795, 2017.

[17] H.-T. Chiu, S. Saito, H. Suganuma, K. Kuriyama, K. Tanaka, H. Hasegawa, T. Miyagi, T. Onizawa, and F. Maehara, "Performance evaluation of MIMO-FTN signaling under multipath fading channels," *IEEE Access*, vol. 11, pp. 89 383–89 392, 2023.

[18] S. Sugiura and L. Hanzo, "Frequency-domain-equalization-aided iterative detection of faster-than-Nyquist signaling," *IEEE Transactions on Vehicular Technology*, vol. 64, no. 5, pp. 2122–2128, 2014.

[19] Y. Yamada, M. Sawahashi, and K. Saito, "Performance of time and frequency compression of faster-than-Nyquist signaling in frequency-selective fading channels," in *2015 21st Asia-Pacific Conference on Communications (APCC)*, 2015, pp. 550–554.

[20] T. Yu, M. Zhao, J. Zhong, J. Zhang, and P. Xiao, "Low-complexity graph-based turbo equalisation for single-carrier and multi-carrier FTN signalling," *IET Signal Processing*, vol. 11, no. 7, pp. 838–845, 2017.

[21] N. Wu, W. Yuan, Q. Guo, and J. Kuang, "A hybrid BP-EP-VMP approach to joint channel estimation and decoding for FTN signaling over frequency selective fading channels," *IEEE Access*, vol. 5, pp. 6849–6858, 2017.

[22] Q. Li, F.-K. Gong, P.-Y. Song, G. Li, and S.-H. Zhai, "Joint channel estimation and precoding for faster-than-nyquist signaling," *IEEE Transactions on Vehicular Technology*, vol. 69, no. 11, pp. 13 139–13 147, 2020.

[23] Y. Ma, N. Wu, J. A. Zhang, B. Li, and L. Hanzo, "Parametric bilinear iterative generalized approximate message passing reception of FTN multi-carrier signaling," *IEEE Transactions on Communications*, vol. 69, no. 12, pp. 8443–8458, 2021.

[24] T. Ishihara and S. Sugiura, "FFT-spread faster-than-Nyquist signaling in frequency-selective fading channel," in *ICC 2022-IEEE International Conference on Communications*, 2022, pp. 2399–2404.

[25] T. Ishihara and S. Sugiura, "Eigendecomposition-precoded faster-than-Nyquist signaling with optimal power allocation in frequency-selective fading channels," *IEEE Transactions on Wireless Communications*, vol. 21, no. 3, pp. 1681–1693, 2022.

[26] T. Ishihara and S. Sugiura, "Reduced-complexity FFT-spread multicarrier faster-than-Nyquist signaling in frequency-selective fading channel," *IEEE Open Journal of the Communications Society*, vol. 3, pp. 530–542, 2022.

[27] Q. Li, F.-K. Gong, P.-Y. Song, G. Li, and S.-H. Zhai, "Joint channel estimation and precoding for faster-than-Nyquist signaling," *IEEE Transactions on Vehicular Technology*, vol. 69, no. 11, pp. 13 139–13 147, 2020.
[28] K. Wang, A. Liu, X. Liang, and S. Pen, "Unique faster-than-Nyquist transceiver of the ACM system," *IET Communications*, vol. 12, no. 4, pp. 432–440, 2018.
[29] S. Wen, G. Liu, C. Liu, H. Qu, L. Zhang, and M. A. Imran, "Joint precoding and pre-equalization for faster-than-Nyquist transmission over multipath fading channels," *IEEE Transactions on Vehicular Technology*, vol. 71, no. 4, pp. 3948–3963, 2022.
[30] T. Ishihara, S. Sugiura, and L. Hanzo, "The evolution of faster-than-Nyquist signaling," *IEEE Access*, vol. 9, pp. 86 535–86 564, 2021.
[31] X. Huang, "Multipath diversity of precoded OFDM with linear equalization," in *2008 IEEE International Conference on Communications*, 2008, pp. 1307–1311.
[32] G. Surabhi, R. M. Augustine, and A. Chockalingam, "On the diversity of uncoded OTFS modulation in doubly-dispersive channels," *IEEE transactions on wireless communications*, vol. 18, no. 6, pp. 3049–3063, 2019.
[33] H. Zhang, X. Huang, and J. A. Zhang, "Adaptive transmission with frequency-domain precoding and linear equalization over fast fading channels," *IEEE Transactions on Wireless Communications*, vol. 20, no. 11, pp. 7420–7430, 2021.
[34] F. Mazzenga and G. Corazza, "Blind least-squares estimation of carrier phase, Doppler shift, and Doppler rate for m-PSK burst transmission," *IEEE Communications Letters*, vol. 2, no. 3, pp. 73–75, 1998.
[35] M. Tong, X. Huang, and J. Andrew Zhang, "Faster-than-Nyquist transmission with frame-by-frame decision-directed successive interference cancellation," *IEEE Transactions on Communications*, vol. 71, no. 8, pp. 4851–4861, 2023.
[36] X. Jiang and F. Kaltenberger, "Channel reciprocity calibration in TDD hybrid beamforming massive MIMO systems," *IEEE Journal of Selected Topics in Signal Processing*, vol. 12, no. 3, pp. 422–431, 2018.
[37] J. M. Nieminen and L. Muche, "A random matrix model whose eigenvalue spacings are closely described by the brody distribution." *Acta Physica Polonica B*, vol. 48, no. 4, 2017.
[38] A. Edelman, "Eigenvalues and condition numbers of random matrices," *SIAM Journal on Matrix Analysis and Applications*, vol. 9, no. 4, pp. 543–560, 1988.
[39] ETSI, ETSI TR and ETSI, TR, "138 901 v15. 0.0-5G; Study on channel model for frequencies from 0.5 to 100 GHz (3GPP TR 38.901 version 15.0. 0 Release 15)," Technical Report, ETSI, Tech. Rep., 2018.
[40] F. M. Dekking, *A Modern Introduction to Probability and Statistics: Understanding Why and How*. Springer Science & Business Media, 2005.
[41] J. G. Proakis and M. Salehi, *Digital Communications*. McGraw-Hill, 2008.